Coastal Engineering 43 (2001) 247–263

Coastal Engineering
An International Journal for Coastal, Harbour and Offshore Engineers

www.elsevier.com/locate/coastaleng

Waves at Holderness from X-band radar

J. Wolf *, P.S. Bell

Proudman Oceanographic Laboratory, Bidston Observatory, Birkenhead, Merseyside CH43 7RA, UK

Received 26 September 2000; received in revised form 26 April 2001; accepted 11 May 2001

Abstract

During the Holderness Experiment of 1994–1995 and 1995–1996, data were collected by a coastal deployment of an X-band radar with simultaneous deployments of various moored and bottom-mounted wave measurement devices. The radar data consist of sequences of images of the sea surface at intervals of 1.5 h over several months. Three-dimensional wave number-frequency spectra were derived from the sequences of captured images using an analysis method developed by Young et al. [J. Geophys. Res. 90(C1) (1985) 1049]. Some aspects of this analysis were refined. An empirical transfer function was derived relating the radar image spectra to the wave spectra measured by other instruments. A new calibration procedure for obtaining wave height from the radar spectra was also derived. The radar spectra were compared with directional spectra collected by a bottom-mounted InterOcean S4DW directional wave-current meter and with Datawell Waverider data. The capabilities of X-band radar in a coastal situation are discussed including the derivation of water depth required to optimise the analysis.

Keywords: X-band radar; Wave measurement; Nearshore waves; Holderness

1. Introduction

The Holderness Experiment was designed to monitor the processes of sediment transport along the UK. Holderness coastline on the North Sea, which is rapidly retreating and provides the largest single coastal source of sediments to the North Sea (Prandle et al., 1996). The morphology of this coastline is described in Pethick and Leggett (1993) who discussed the importance of waves in the net transport of sediment. They stated that waves with return periods of 8–15 months contribute to a net southerly transport while waves of more frequent occurrence (and lower energy) have no net transport. Waves of longer return periods, which are less frequent and more extreme events, tend to develop offshore bars. Various processes have an impact on sediment transport including tides, storm surges and waves. Breaking waves have a particularly important impact on the beach and in the nearshore zone and the direction of approach is critical for determination of the longshore drift current and net sediment transport. However, it is difficult to make directional wave measurements using standard instruments in very shallow water, e.g. the Datawell Directional Waverider buoy requires depths greater than about 10 m for the recommended compliant mooring to reduce mooring interference effects. Alternative methods are needed such as bottom pressure recorders and remote-sensing devices like the coastal X-band radar described here.

* Corresponding author. Fax: +44-151-653-6269.
E-mail addresses: jaw@pol.ac.uk, jawpsb@pol.ac.uk (J. Wolf), psb@pol.ac.uk (P.S. Bell).

0378-3839/01/$ - see front matter
PII: S0378-3839(01)00016-3

Wave data were collected during the winters of 1994–1995 and 1995–1996. Sea level and profiles of suspended sediment and currents were also measured. Wave measurements were made at several stations using conventional in situ instruments: the InterOcean S4DW (Directional Wave) wave-current meters, pressure wave recorders and Datawell Waverider buoys (directional and non-directional), and also by remote sensing: satellite altimeter and SAR, HF radar and X-band radar. The data set is of interest in providing a large synoptic data set for the study of waves in shallow water (Wolf, 1998) and for the intercomparison of the different wave measuring techniques, which was carried out in the EC SCAWVEX project (Wolf, 1996; Krogstad et al., 1999). Although there were rather few high wave events during this period (the prevailing westerly winds generate fetch-limited wind-sea combined with long period swell), significant wave heights exceeded 3 m on five occasions in the first experiment (winter 1994–1995) and four occasions during the second experiment (winter 1995–1996). The wave frequency distribution showed larger significant wave height and peak wave period for waves coming from the directions NE and SE (Wolf, 1998).

In Section 2, we discuss the analysis of radar images for waves in general. In Section 3, the data collection procedure is described. Section 4 gives details of the analysis procedure used for the Holderness X-band radar data, with results, discussion and conclusions in Sections 5, 6 and 7, respectively.

2. Analysis of radar images of waves

The use of a rotary scanning marine X-band radar for obtaining images of sea waves has been developed over many years. Some references to this work are, e.g. Heathershaw et al. (1980), Young et al. (1985a,b), Ziemer and Rosenthal (1987), Ziemer (1991), Proctor and Wolf (1991), Borge et al. (1999) and Reichert et al. (1998). The radar backscatter mechanism is generally assumed to be mainly resonant Bragg-scattering at near grazing angle incidence from the waves with the wavelength related to the radar wavelength. This mechanism seems to explain features of the backscatter of longer radar wavelengths, e.g. HF ground-based radar (Wyatt et al., 1999). For waves approaching with crests perpendicular to the radar the Bragg-resonant waves would have wavelength $\lambda_w = \lambda_R/2$ (where λ_R is radar wavelength ~ 3 cm for X-band), giving a wavelength of about 1.5 cm in the gravity-capillary range (Phillips, 1977). One problem is the shadowing of part of the sea surface by the waves themselves at low incidence angles (as in the case here). The incidence angle and incident radiation will vary with distance from the radar. The longer gravity waves (observed in the image) modulate the short Bragg-resonant waves. Tucker (1991, p. 237) has raised the issue of the persistence of these very short Bragg-resonant waves, which may be less than 1 s. There are several mechanisms, which would contribute to the modulation of the short waves, e.g. hydrodynamic and tilt modulations (see Robinson, 1985). Therefore, the backscatter model is quite complex and some aspects of the empirical results in wave measurement do not agree with accepted theory. It is relatively easy to get estimates of wave number, frequency and direction of the waves but more difficult to quantify the wave height. The radar backscatter cross-section is correlated with the wave height but a calibration coefficient has to be derived for each deployment.

The analysis methodology follows that developed by GKSS (Young et al., 1985a,b; Ziemer and Rosenthal, 1987) with some refinements. The novel aspects lie in the method of calibration of the radar spectra, derivation of the empirical transfer function, determination of water depth and the comparison of the radar wave data with a new data set from conventional wave measuring devices. The radar spectra have been compared with non-directional spectra obtained by bottom-pressure recorder and Waverider at a nearby station N1 and directional spectra measured by a bottom-mounted InterOcean S4DW at the same location. An estimate of the empirical transfer function is derived allowing estimates of the wave spectra to be computed from the image spectra. Various integrated parameters are then derived from these spectra and compared with the conventional observations, finally producing an optimised calibration procedure for this particular radar installation. More work needs to be done to investigate to what extent this calibration may be applicable in other deployments.

3. Data collection

The radar was deployed on the cliff-top at Tunstall on the Holderness coast (53°45.83′N, 00°00.83′W), being the shoreward end of line N1-N3, at a height of approximately 10 m above sea level (see Fig. 1 for instrument layout). The radar system operates at 9.41 GHz with a scan-rotation rate of 2.25 s and pulse repetition frequency of 1200 Hz. The radar wavelength is approximately 3 cm. The sample rate is 20 MHz, the pulse duration 8 μs and 8 pulses are averaged. This gives an azimuth resolution of just over 1° and a range resolution of 4.69 m. From the full PPI (plan position indicator) image, a 600-m^2 box is extracted and interpolated onto 128 × 128 pixels (i.e., 7.5-m spatial resolution). The radar resolution (determined by the hardware, pulse length, etc.), thus, is 0.08986 rad/s in frequency and 0.01055 rad/m in wave number. The shortest wave period directly detectable is about 4.4 s, but the wave number resolution is somewhat better and the equivalent period in deep water for the shortest waves is about 3 s. For an antenna height of 10 m, the angle with the vertical is 89.2° at 700-m range.

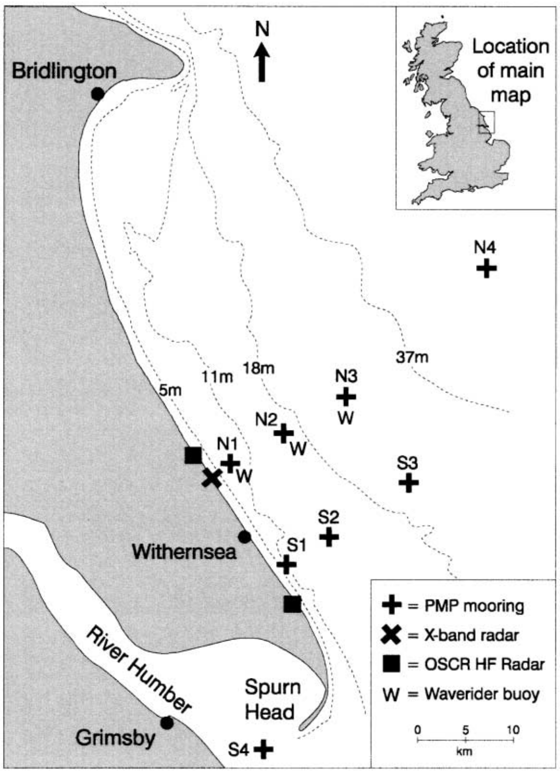

Fig. 1. Holderness experimental layout.

Table 1
Days on which radar data are available

Date
6–9 October 1994
13–14 October 1994
20–22 October 1994
26–30 October 1994
3–11 November 1994
17–18 November 1994
5–20 December 1994
22 December 1994
24–28 December 1994
30 December 1994–2 February 1995
20–24 February 1995
26–27 February 1995
1–2 March 1995

The hardware, data collection software and logistical problems are discussed in Bell and Hardcastle (1996) and Bell (1998). An important problem is the alignment of the antenna. No absolute measure of the orientation was made in this experiment. It would be desirable to use a radar reflector deployed at a known location to calibrate the azimuth in a subsequent deployment. Wave directions were adjusted by a constant angle after comparison with the wave direction measured by S4DW at N1 (see Section 5.3). The water depths over the radar footprint are required for proper analysis of the wave data. A fine-scale bathymetric survey of the area was not available, however, the S4DW also measures total water depth and this was used in the analysis together with a radar-derived estimate of water depth (Section 4.3).

The system was programmed to collect a sequence of 32 scans every 1.5 h, plus an extra data capture close to predicted high water. The duration of the data capture was thus about 1 min. The days for which data exist in 1994–1995 (although the data are not necessarily complete for each day) are shown in Table 1. Non-directional Waverider (WR) data at N1 are available from 9 October 1994 to 28 February 1995 at 1.5-h intervals and directional S4DW data at hourly intervals for 9 October–8 November 1994, 10 November–31 December 1994 and 16–30

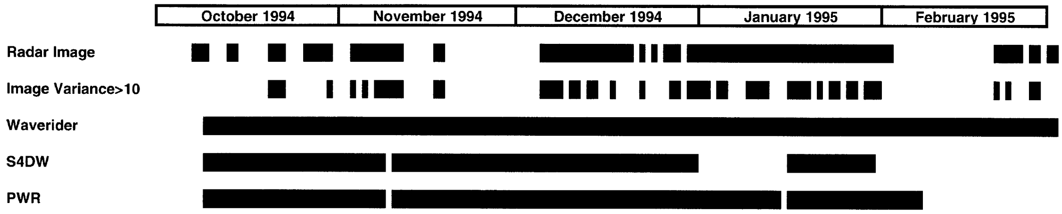

Fig. 2. Bar chart for data coverage: radar, Waverider, S4DW and PWR. The first two horizontal lines represent (a) whether a radar image was captured and (b) whether the variance was sufficient for successful wave analysis.

January 1995. The total number of radar images processed was 1245. Of these, 1144 coincided with WR data and 373 had both WR and S4DW spectra obtained (almost) simultaneously (i.e., within 0.5 h). Another bottom pressure instrument, the pressure water-level recorder (PWR) also gave water depth and non-directional wave spectra at N1. The data availability is shown graphically in Fig. 2.

An example of a radar PPI image is shown in Fig. 3 for 12:00, 1 January 1995. This is in polar coordinates (range and azimuth) with the intensity related to the ratio between incoming and outgoing energy. The darker grey indicates a higher backscatter signal. This illustrates how a clear image of long waves is obtained although the imaging mechanism is not fully understood. The largest waves observed during the whole Holderness experiment were on 2 January 1995. The highest waves recorded by all three wave measurement devices simultaneously (i.e., radar, WR and S4DW) were at 09:00, 26 January 1995.

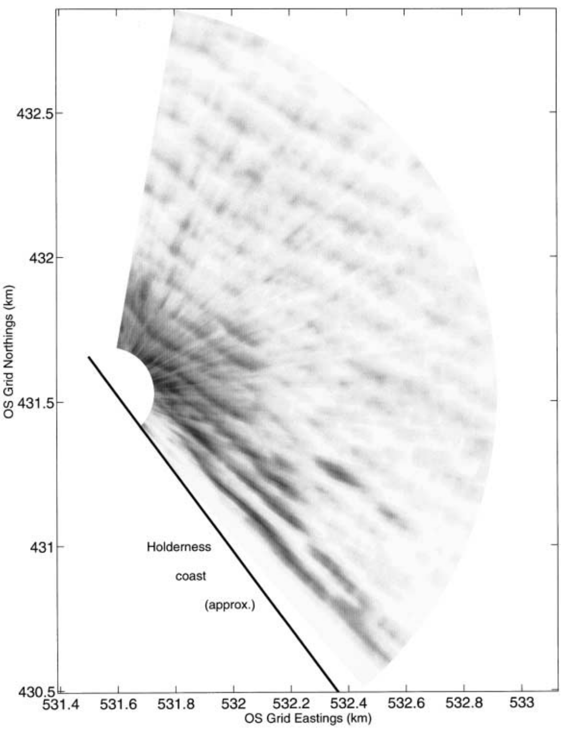

Fig. 3. Radar PPI image with sea-clutter, showing surface waves (darker grey indicates strongest backscatter) for 12:00 on 1 January 1995 at Holderness.

4. Data analysis

4.1. Spectral analysis

The analysis followed the basic method developed by GKSS (i.e., Young et al., 1985a; Ziemer and Rosenthal, 1987). A consecutive sequence of 32 images is captured. For each image, a 600×600 m^2 is extracted with 7.5-m grid resolution. The maximum range of the radar is about 1.35 km offshore; the part of the image that is analysed lies inshore of this. Each set of 32 scans was processed by use of a three dimensional fast Fourier transform to produce a wave number frequency spectrum. This may be termed the image spectrum, $I(k_x, k_y, f)$ in which 17 positive frequencies, f, (equally spaced from 0 to 0.23 Hz) are resolved and 128 wave numbers in each direction in Cartesian (x, y) space, k_x and k_y. The peak of the energy is identified in wave number space for each frequency. The variation of energy over several frequency planes is shown in Fig. 4. In this figure, the x and y axes represent the wave number space for the first 61×61 wave numbers (at most, 2–3% of the total variance is lost by cutting off the higher wave numbers). The contours are of

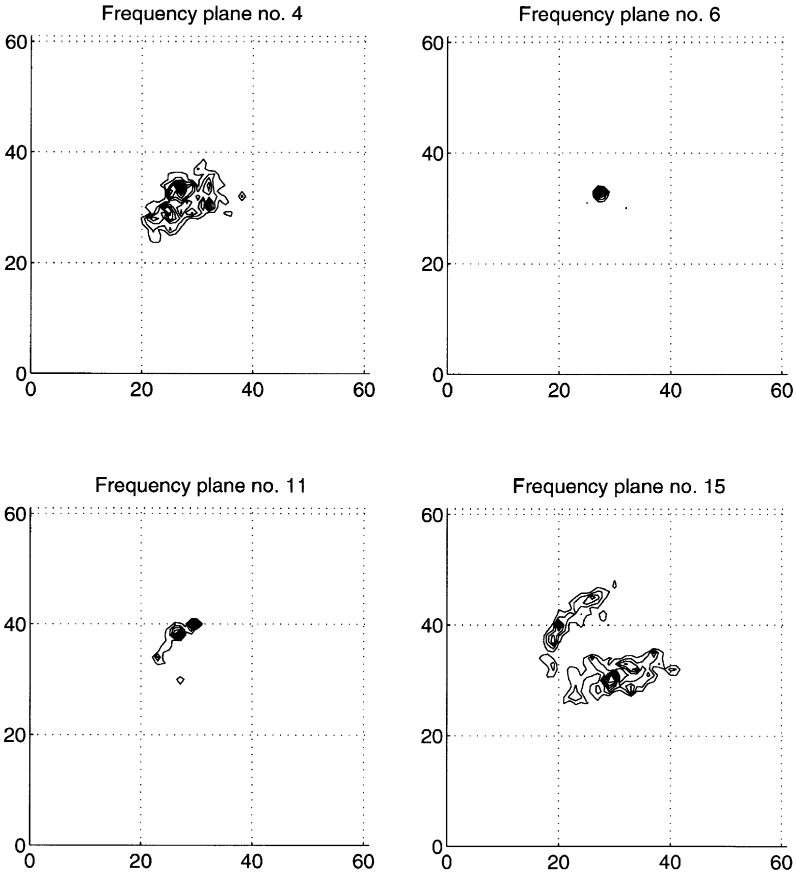

Fig. 4. Image spectral energy in each of four frequency planes showing distribution of energy in wave number space.

the image energy in arbitrary units. The lower and higher frequency planes are very 'noisy' with multiple peaks in wave number space. Thus, it is difficult to resolve the main wave-related peak. There may also be higher harmonics of the dominant peak.

The resolution in wave number space is better than in frequency, so the average of the frequency planes is used to give a 2D wave number (k_x, k_y) spectrum, which is then converted to the frequency and direction (f, θ) spectrum using the linear dispersion relation. The latter requires knowledge of the ambient depth and current. An example of the observed vs. theoretical dispersion curve for 12:00, 1 January 1995, is shown in Fig. 5. It may be seen that the peak wave number (i.e., the wave number corresponding to the peak energy for a given frequency), extracted for each frequency plane, falls on or close to the linear dispersion curve for frequencies 6–13 (for discrete points along the frequency-axis, where frequency 1 corresponds to zero). This is as observed in Young et al. (1985a,b). For the lowest and especially the highest frequencies, the peak wave number can be quite far removed from the linear dispersion curve. However, for the frequencies corresponding to the peak of the wave spectrum (periods 6–14 s), the linear dispersion relationship appears to hold. What we want to know is how much information about the 'real' wave spectrum can be obtained from the image spectrum derived above.

The first analysis carried out on the Holderness 1 data showed promising results but identified some problem areas (Bell and Hardcastle, 1996). Their analysis gave useful results for wave direction and generally good identification of peak frequency,

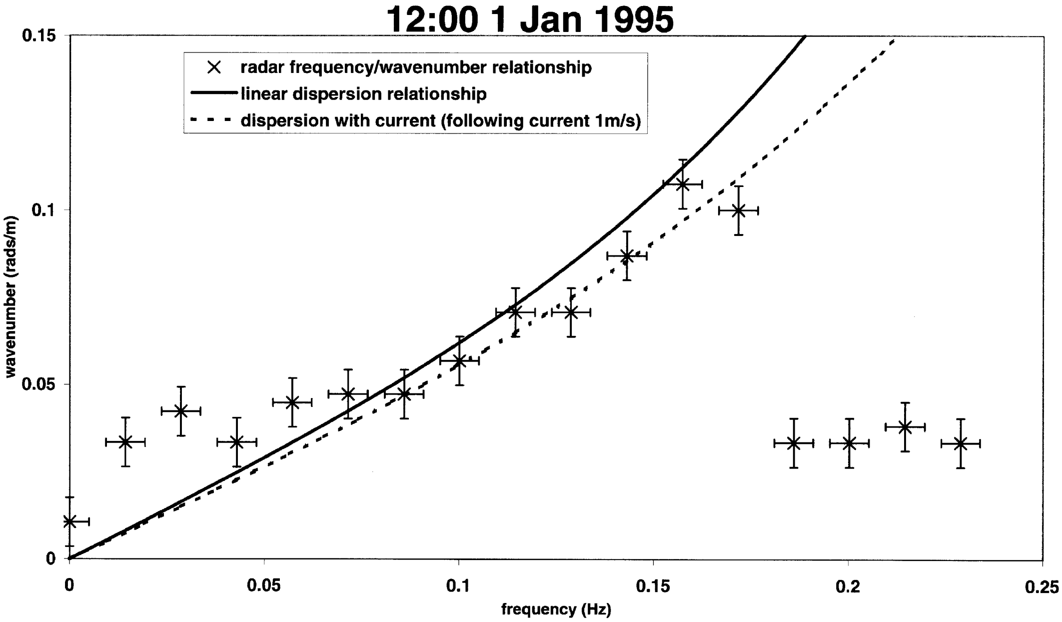

Fig. 5. Radar peak wave number identified in each frequency plane, plotted against frequency, compared with linear dispersion curves with and without current. Error bars on the radar points show the resolution with which the frequency and wave number can be defined.

however, the wave height information derived was poor (using only the total backscattered energy gave poor correlation with wave height measured by a pressure sensor). They found that the best returns (i.e., maximum back-scattered energy) were obtained from the analysis of the most near-shore part of the radar image. In the following sections, we examine the advantages and disadvantages of selecting the near-range or far-range part of the image, the quality control procedures and depth determination needed to optimise the analysis and an improved wave height estimation using an empirical transfer function to convert the image spectra into equivalent wave spectra.

4.2. Quality control

It is important to select images with sufficient variance (or contrast) for the analysis procedure. This is affected by the gain setting on the radar but the latter has to be left constant after setup to allow comparison of the derived wave heights. The grey-scale digitisation gives a maximum dynamic range (8 bits) of 0–255. An image variance greater than 10 was found to be a suitable threshold for analysis. This eliminated times of very low wave height and greatly improved the comparison of derived wave parameters such as wave height with those from other instruments (see results in Section 5). About 50% of the images had sufficient contrast in the images to be suitable for analysis (623 occurrences). This information is summarised in the bar chart in Fig. 2.

Another method of improving the noise-signal ratio is to use the ‘noise-reduction’ option, developed by GKSS, where only energy ‘close’ to the linear dispersion shell is retained. The effect of an ambient current will displace the dispersion shell but, as shown in Fig. 5, even a large current of 1 m/s will still fall within the error bars of the frequency-wave number resolution of the radar. Therefore, the radar does not appear sensitive enough to allow accurate determination of the current. In the analysis, the observed S4DW current was included when available, but was found to make a negligible difference in the results.

4.3. Depth determination

The water depth must be supplied to the wave analysis routine (see Section 4.1). If no other information is available, an estimation of the water depth, h, can be obtained by calculation from the linear dispersion relation for the overall spectral peak in wave number-frequency space, k_P, ω_P; where $\omega_P = 2\pi f_P$, $k_P = \sqrt{\left(k_{xP}^2 + k_{yP}^2\right)}$:

$$h = \frac{1}{2k}\ln\left(\frac{gk_P + \omega_P^2}{gk_P - \omega_P^2}\right), \text{provided that } gk_P > \omega_P^2 \quad (1)$$

The errors in this estimate are quite large, due to the rather coarse frequency and wave number resolution and increase with water depth. For example, the error is up to ± 2.5 m for $h = 10$ m.

If time-variation can be ignored, waves propagating over spatially varying water depth will have a constant frequency but the wave number will change. In the spectral analysis (Section 4.1), the effect of large depth variations over the image would be a smearing of energy over a large wave number band leading to an equivalent smearing in frequency, poor determination of peak period and large errors in integrated spectral parameters. Ideally, we want an area of constant depth within the radar footprint. For this reason, the far-range rather than the very nearshore part of the radar image is preferable for the analysis. The tidal range in the Holderness region is about 5 m and must also be taken into account (e.g., error in depth of 5 m in 10 m could lead to error of 0.02 Hz in frequency for the energy-containing frequencies at ~ 0.1–0.2 Hz). An initial analysis of all the radar data was made, using a first guess for the depth, $h = 10$ m, and zero current. The radar analysis was repeated for the images with coincident S4DW data, using S4DW depth and currents and rotation of the wave direction to give best agreement in direction. The data, at 3-h intervals, produced 373 spectra, of which 185 were suitable for analysis (i.e., sufficient variance in image). Using a better estimate of depth (including tidal variation) improved the analysis (as measured by the better agreement of radar estimates of wave parameters with those measured by the other instruments.

4.4. Derivation of empirical transfer function

The radar image spectra were compared with observed directional spectra from the S4DW and non-directional WR spectra at N1, in order to derive an empirical transfer function, which can then be used to convert the image spectra to wave spectra and perhaps gain some insight into the imaging mechanism. The spectra were compared in a systematic fashion by computing a spectral ratio at each frequency (Wolf, 1996). A bias-free estimate of this, $r(f)$, is given by:

$$r(f) = \frac{S_Y(f)(\nu_X - 1)}{S_X(f)\nu_X} \quad (2)$$

where ν_X is the number of degrees of freedom (df) associated with the spectral estimate $S_X(f)$. Here, either the WR or S4DW spectra, and $S_Y(f)$ is the radar spectra. For the WR and S4DW spectra, the df was 10 or 20 depending on frequency resolution and amount of averaging of the raw spectra. The various spectra were interpolated onto a standard set of frequencies and the ratio computed.

Ziemer and Rosenthal (1987) determined an empirical transfer function by optimising the fit of significant wave height, H_S, and zero-up-crossing period, T_Z, using a constant multiplier and a power of frequency. Here, we use the spectral ratio to derive a transfer function. We can define a transfer function $T(f)$ such that:

$$T(f) = E(f)/I(f) \quad (3)$$

where $E(f)$ is the spectrum of the actual sea surface waves. Several different options for the transfer function are listed in Table 2. The constants A and a were adjusted to give the best agreement of mean spectra in each case. After conversion of the image spectra to pseudo-wave spectra and a tail-fitting procedure applied above 0.17 Hz, the spectra were integrated to give standard spectral parameters.

Table 2
Transfer functions tested

Option number	$T(f)$	Correlation (H_{Sr}, H_{Sw})	r.m.s. (H_S) (m)	Offset Offset
0	A	0.751	0.35	0
1	Af^2	0.782	0.32	0
2	$A\tanh^2(kh)$	0.779	0.33	0
3	$AI(f)$	0.649	0.40	0.64
4	$AI(f)f^2$	0.709	0.37	0.58
5	$AI(f)f^4$	0.798	0.31	0.46
6	$AI(f)f^5$	0.802	0.31	0.45
7	$AI(f)f^6$	0.795	0.32	0.45
8	$AI(f)\exp(af)$	0.793	0.32	0.45

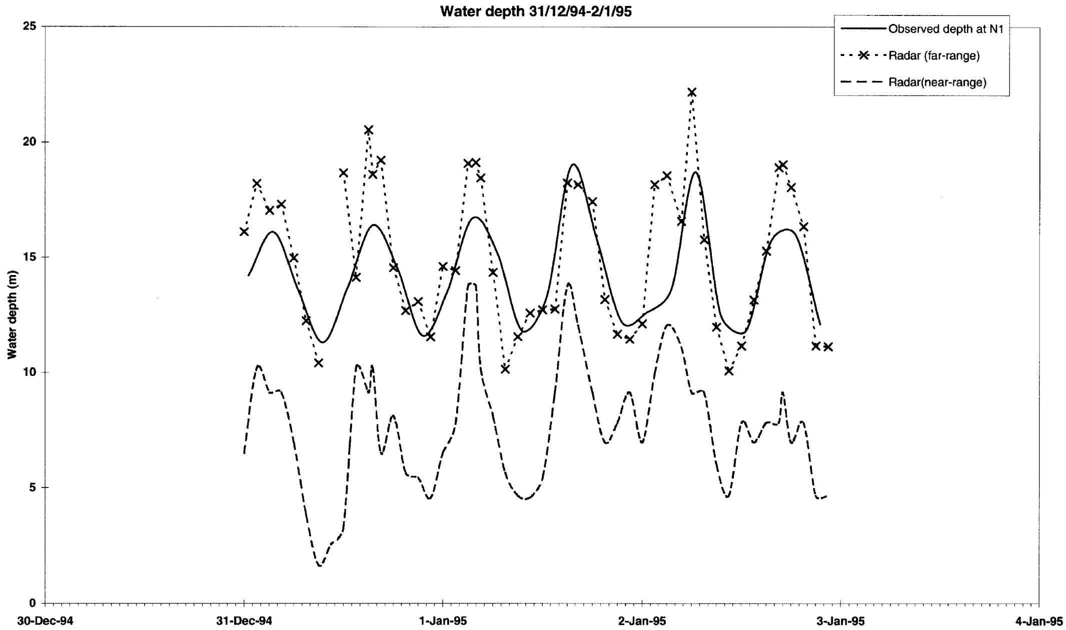

Fig. 6. Near- and far-range radar depths at Holderness, compared to observed depths for 31 December 1994–2 January 1995.

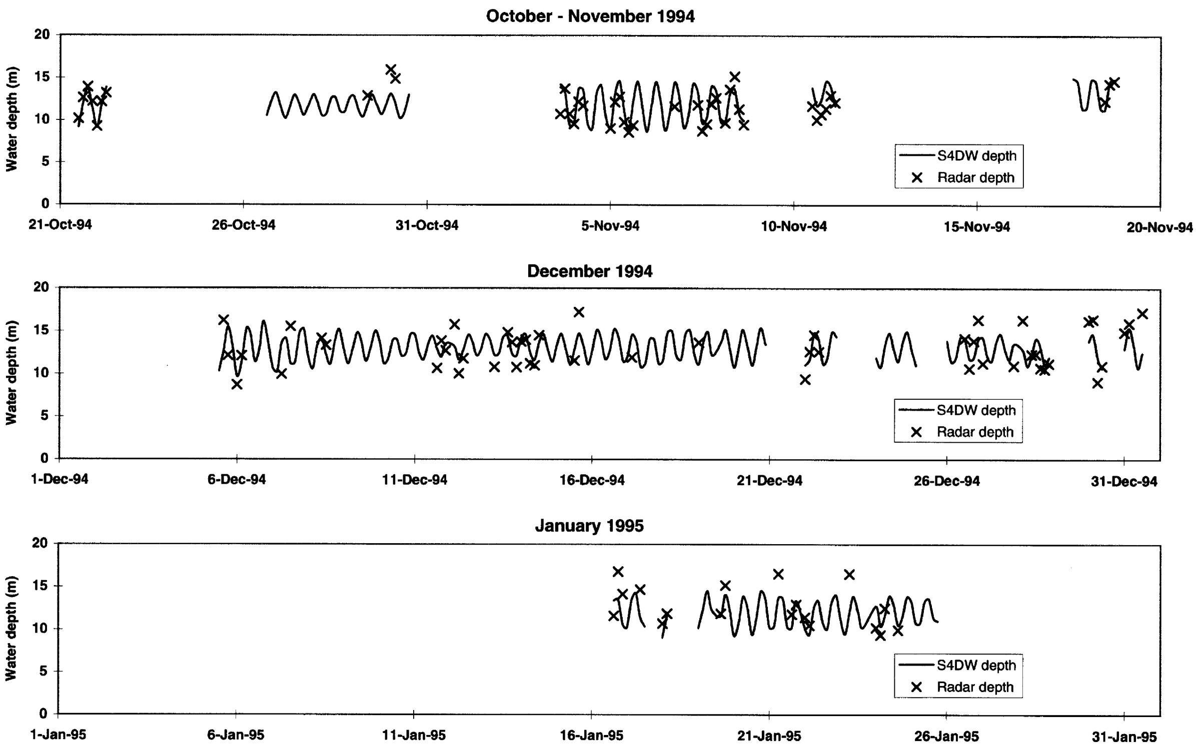

Fig. 7. Depth time series—comparison of radar estimates with observed depths for whole deployment.

5. Results

5.1. Radar estimates of water depth

The observed water depth has been plotted for 31 December 1994–2 January 1995 for the near-range (150–750 m) and far-range (700–1300 m), as shown in Fig. 6. Simultaneous depths, measured at a location (N1) just offshore of the radar image by a bottom-mounted pressure recorder (PWR) were used to provide a time history of water depth, which appeared to be a good approximation to the water depth for the far-range image region. The mean depth over the far-range was calculated as 15.3 m from the radar and 14.2 m by the PWR. The mean depth in the near-range is about 7.7 m, i.e. the near-range depths are approximately 7 m shallower than at N1. Improved agreement is obtained by using a parabolic interpolation function to determine the peak of the spectrum. Since the far-range depths appeared to be in good agreement with the depths at N1, and the spatial variation in depth is likely to be less offshore, the far-range part of the image was used in subsequent analysis. As discussed earlier, the depth estimation has large error bars with an error of over 2 m in 10 m of water. Therefore, this is only a qualitative check that the wave number and frequency at the peak of the image spectrum do agree with linear wave theory and not a way of determining depth to any degree of accuracy. More effective ways of using X-band radar for bathymetric mapping are discussed in Bell (1998, 1999).

The depths computed for the full Holderness 1 period are compared with S4DW depths in Fig. 7. Fig. 8 is a scatter plot of the same data. Of the 185 images, 134 produced an estimate of the water depth

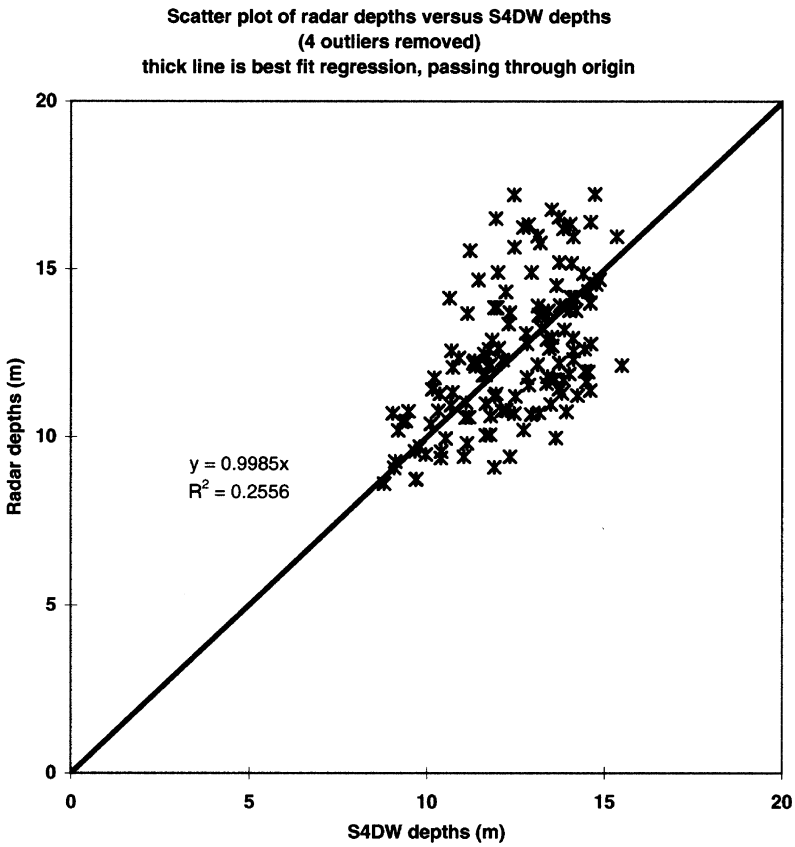

Fig. 8. Depth scatter plot for data as shown in Fig. 7.

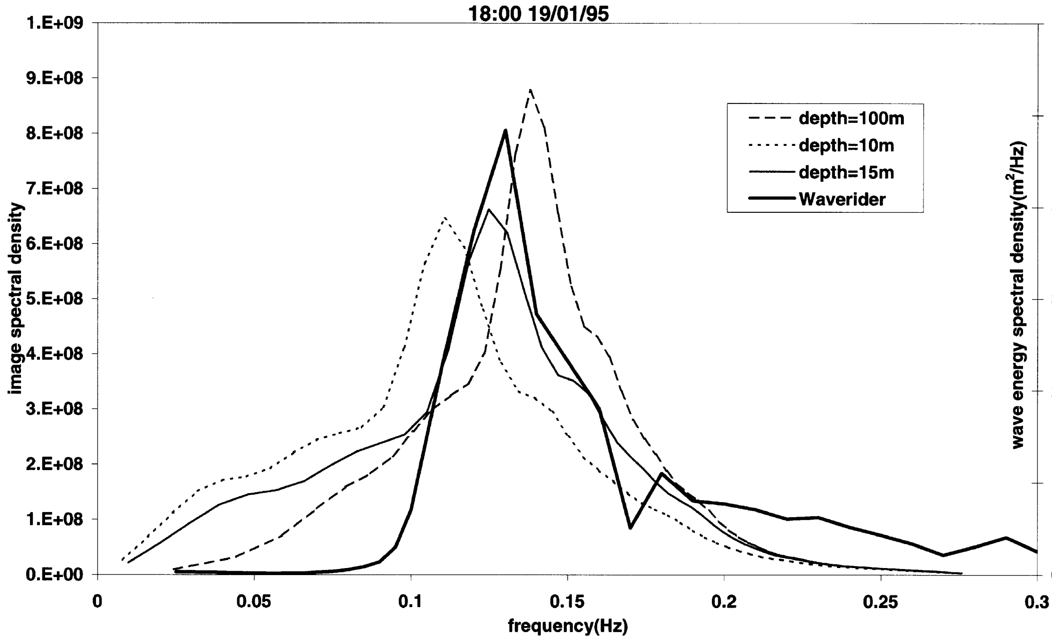

Fig. 9. Illustration of effect of depth on analysis for spectra at 18:00 on 19 January 1995.

from the energy maximum. The mean depth derived from these was 12.5 m, in close agreement with the S4DW mean depth over the whole deployment. However, there is a large amount of scatter, making the individual estimates of depth not reliable. Since there is good agreement between the mean radar-

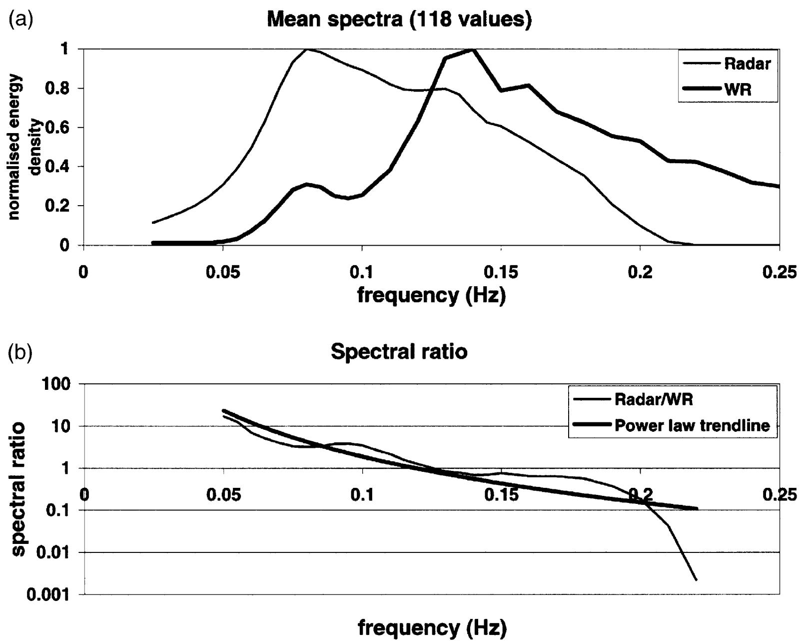

Fig. 10. Energy spectra, radar vs. Waverider (a) mean spectra and (b) spectral ratio.

estimated depths and the observed depths at N1, the latter was assumed to be reasonably representative of the depths over the far-range footprint of the radar. The S4DW depths were therefore used, when available, in the analysis. When these were not available, a mean depth of 12.5 m was used to analyse the remainder of the data for comparison with the WR observations.

Fig. 9 shows the effect of using different depths in the analysis, shifting the main spectral peak in frequency (due to the conversion from wave number space). A water depth of 100 m represents deep-water wave conditions. At this instant, there is a clearly defined single peak in the spectrum. Reducing the depth to 15 m brings the spectral peak to a lower frequency (in better agreement with the WR). A further reduction to 10 m lowers the frequency further but also broadens the peak significantly. It is obviously desirable to use accurate depths when possible.

5.2. Transfer function

Spectra for all coincident data have been compared with (directional) S4DW and (non-directional) WR data measured at N1. In Fig. 10, we see the comparison of the radar and WR spectra, for the times when S4DW depths were available. The (normalised) mean spectra for radar and WR are in Fig. 10a. Fig. 10b is the spectral ratio, plotted on a logarithmic scale; the trend line through this is well fitted by a power of frequency. On average, the peak in the radar spectra is shifted to lower frequency. We can see that the radar spectra are only resolved up to 0.22 Hz and above about 0.17 Hz, the energy drops off rapidly. If the trend line is fitted between 0.05 and 0.17 Hz, the best fit is proportional to $f^{-2.6}$.

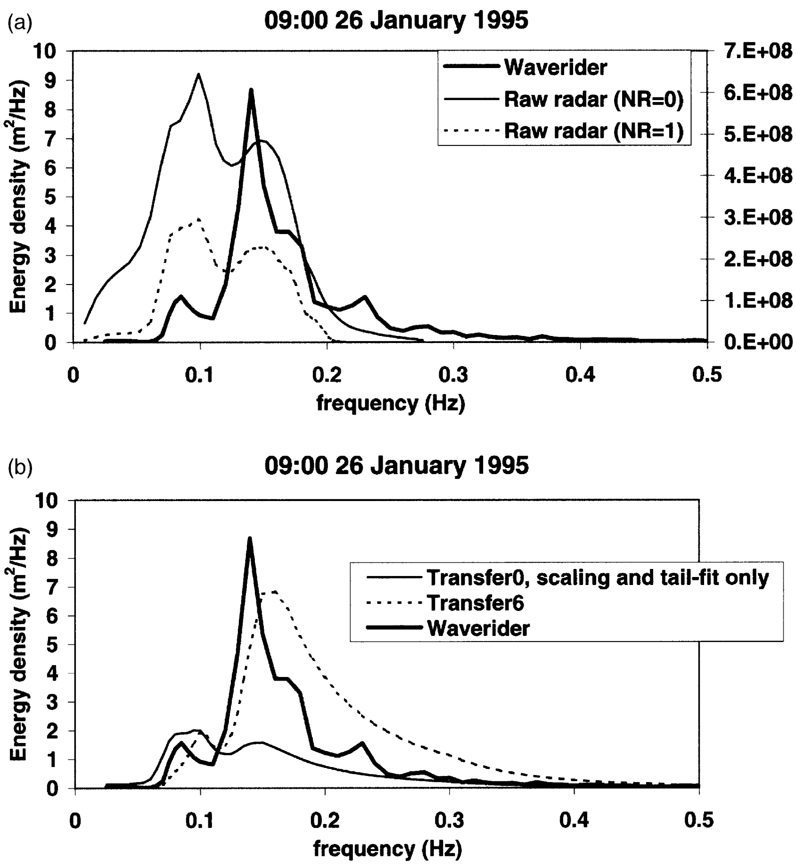

Fig. 11. Energy spectra—effect of (a) noise reduction and (b) transfer function.

It was found that better agreement with the significant wave height observed by the Waverider was obtained if the image spectrum was squared, leading to further options for the transfer function as a function of the image spectrum itself (Table 2, options 3–8). Options 3–8 also required an offset correction for bias to give optimum correlation (see Table 2). The best fit was finally obtained with option 6 using the image spectra squared and frequency to the power 5.

The effect of using the noise reduction option (see Section 4.2) can be seen in Fig. 11a for one spectral realisation at 09:00 26 January 1995, which is the time of maximum wave height recorded by all 3

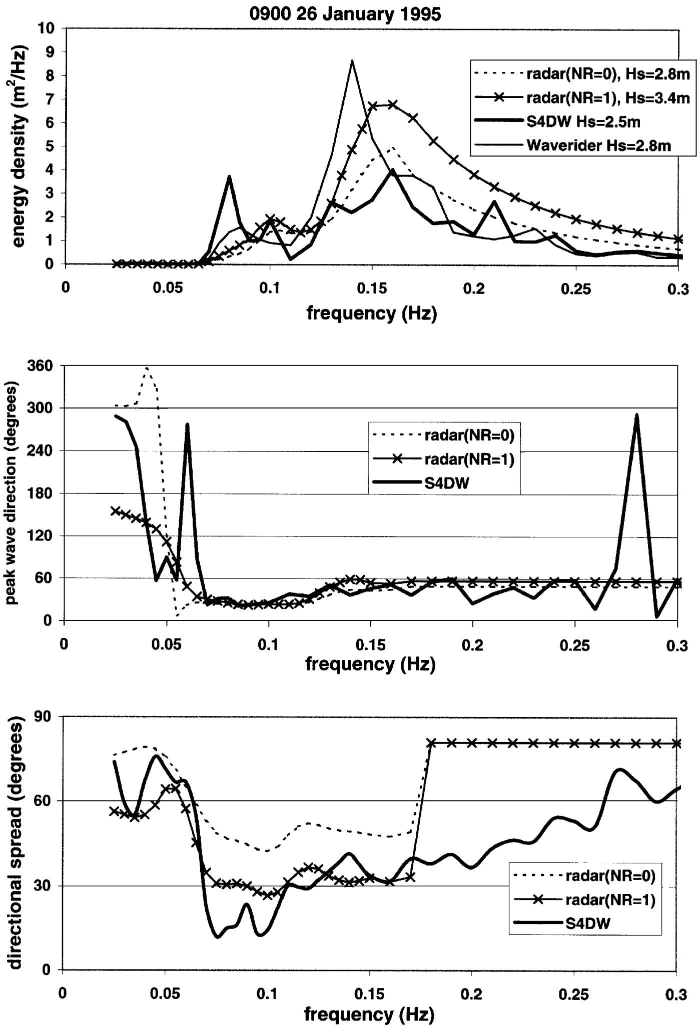

Fig. 12. Comparison of radar directional spectrum, with and without noise reduction at 09:00, 26 January 1995, with Waverider and S4DW.

instruments. The noise reduction, (NR = 0 is no noise reduction, NR = 1 includes noise reduction) cuts out a significant proportion of the image variance without changing the spectral shape significantly. The best fit transfer function, $AI(f)f^5$, is shown in Fig. 11b. Fig. 12 shows more details of the converted spectrum for the same time including peak wave direction and directional spread for each frequency. It also illustrates the differences that occur between other conventional wave measuring instruments, viz. WR and S4DW, making it difficult to decide which option gives better agreement in the

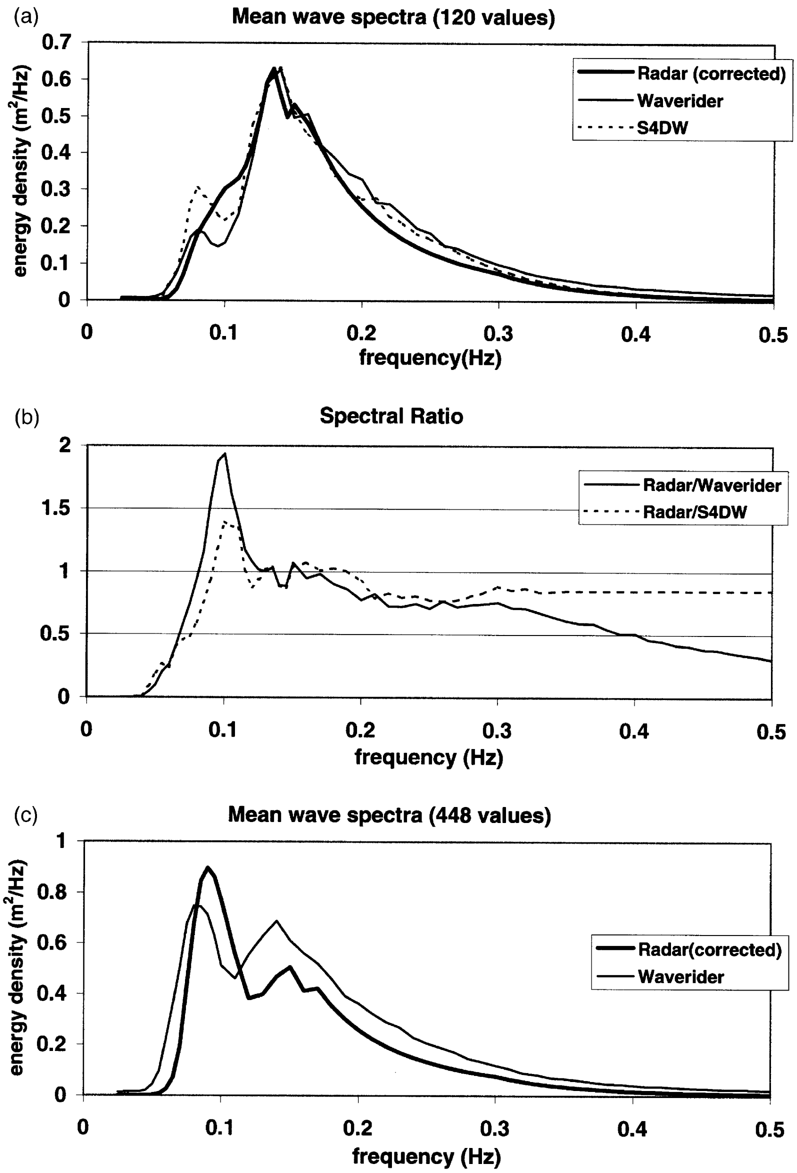

Fig. 13. Mean wave spectra and spectral ratio for whole deployment: (a) S4DW, WR, radar; (b) Spectral ratio; (c) Waverider (constant depth analysis).

energy spectrum at this time. The inclusion of noise reduction appears to improve the agreement in directional spread.

Fig. 13 shows the final result for mean spectra and spectral ratio after application of the optimum transfer function. Multiplying by a frequency-related transfer function shifts the peak of the spectrum. Fig. 13a shows the mean spectra for all simultaneous spectra and Fig. 13b shows the spectral ratio for radar vs. WR and S4DW data, which illustrates the differences between WR and S4DW spectra (discussed in Wolf, 1996). The ratio is closer to unity for the S4DW data. In Fig. 13c, the analysis has been extended to cover all simultaneous WR data using a constant depth. The agreement of the mean spectra is poorer than in Fig. 13a.

5.3. Radar estimates of integrated wave parameters

It is usual to compare different wave measurements using integrated spectral parameters such as significant wave height and period. Peak period and direction are also commonly used. Bell and Hardcastle (1996) carried out a comparison of the peak wave direction from the radar with the peak direction measured by the Directional Waverider at N2 (further offshore than N1) throughout the Holderness deployment. The radar directions were closer to the perpendicular to the coastline, consistent with refraction by the shoaling depths. In addition, comparisons of individual frequency spectra with beach pressure transducers were made, which showed reasonable qualitative agreement. We now examine different methods of estimating wave height, which was seen as more problematic.

5.3.1. Determination of significant wave height from image variance

There is an obvious correlation between the image variance (i.e., total backscatter energy) and the observed wave height (see Bell and Hardcastle, 1996). Two parameters of the image intensity were investi-

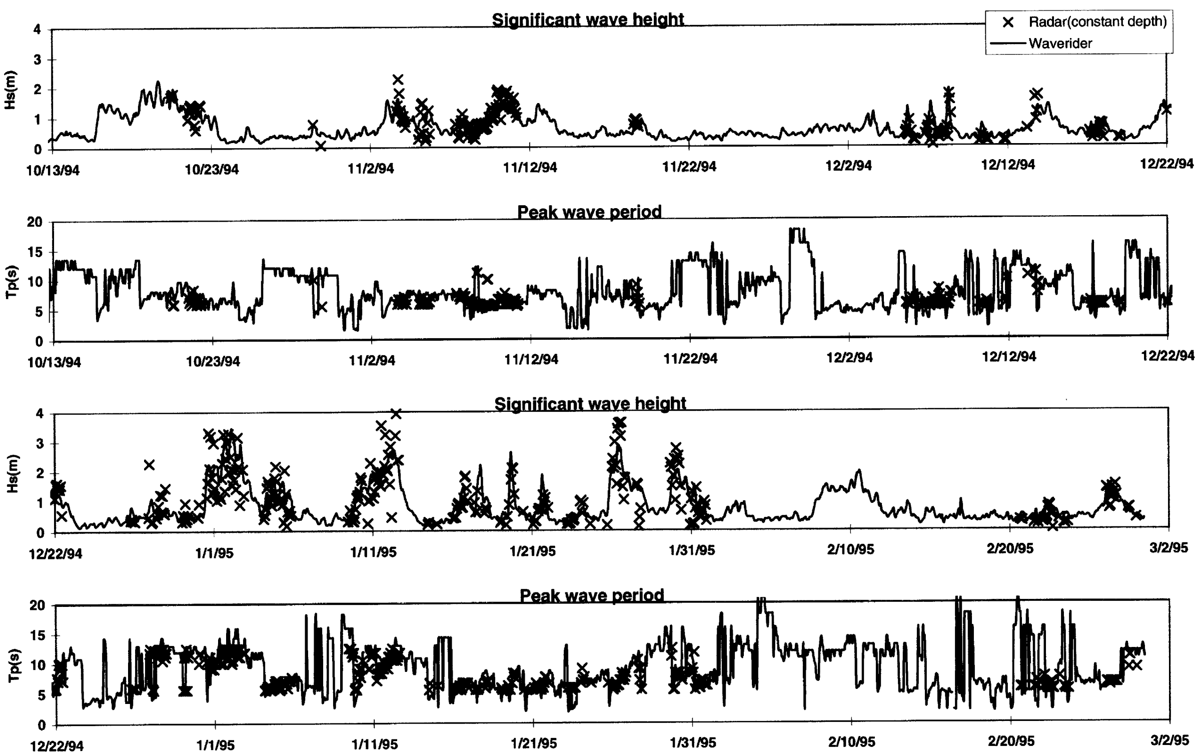

Fig. 14. Time series of significant wave height and peak period for whole deployment comparing radar and Waverider.

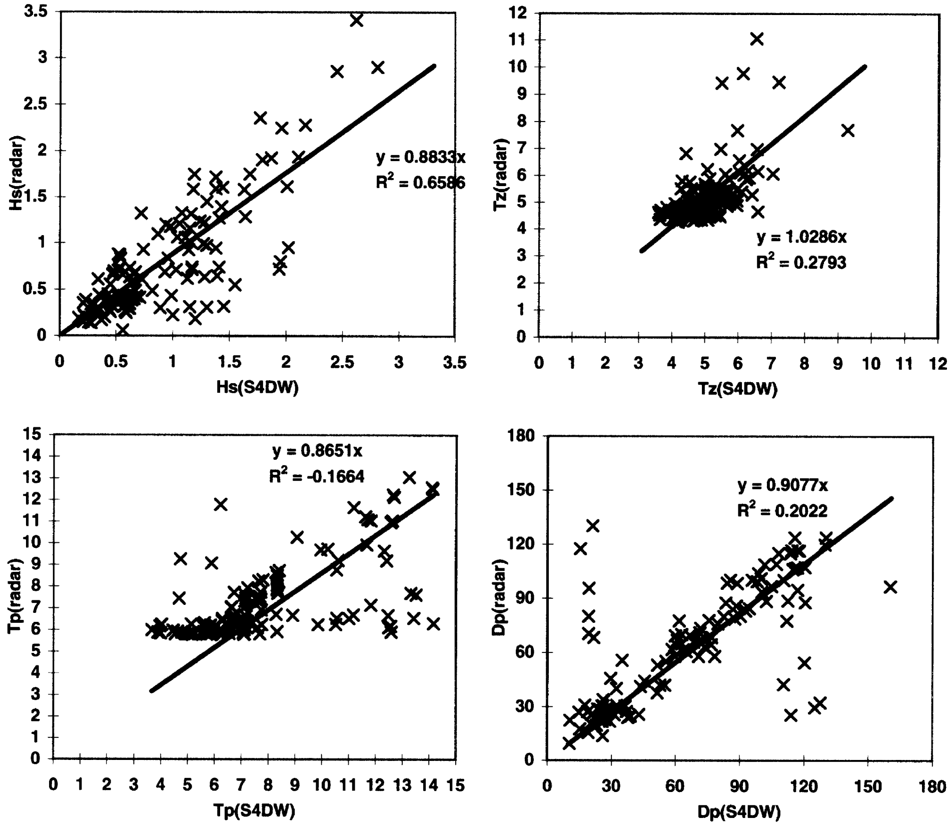

Fig. 15. Scatter plots for radar vs. S4DW data: H_S, T_z, T_P and D_P.

gated: the total variance, E_{tot}, and the peak of the image spectral density, I_{max}. The latter gave better correlation, but the best correlation was with $(I_{max})^{1/4}$. Borge et al. (1999) have developed a method of deriving wave height from the signal to noise ratio of the wave spectra. This method has not been attempted here.

5.3.2. Integration of corrected spectra

After the transfer function has been applied, the radar wave spectra can then be integrated to give parameters such as significant wave height and period. These show better agreement with the independent estimates of the same parameters than the raw image estimates of wave height from Section 5.3.1 (see Table 2). Note that in order to obtain best agreement with the S4DW data, the wave directions were rotated by 073°.

The time series of wave height and peak wave period for constant water depth are shown in Fig. 14 compared with the WR observations. The agreement is better when the S4DW depths are used but less data points can be calculated. The peak wave direction follows the S4DW data very closely. Scatter plots of wave height, period and direction are given in Fig. 15. The agreement in wave height and direction is better than in wave period. The radar used here cannot resolve wave periods shorter than about 6 s.

6. Discussion

The full mechanism of microwave radar backscatter at low (grazing) incidence is not known. An empirical transfer function between the image spectra and wave spectra has been derived here for the simultaneous WR, S4DW and radar spectra. From the transfer function, it may be seen that the radar returns much more backscattered energy at low frequencies (below the spectral peak) than at high frequencies, where a rather sharp cutoff is observed. The transfer function is best fitted as a power of the frequency. This does not agree with theory for the Bragg scattering model, which depends on the modulation of the Bragg-resonant waves by the longer waves imaged by the radar. If the hypothesised hydrodynamic and tilt modulation mechanisms are important, then the controlling parameters would be expected to be wave slope and orbital velocity. Both these mechanisms would amplify the backscatter at higher frequencies—here, the lower frequencies are amplified. From the images, the forward face of the longer waves appears more reflective to radar energy than shorter waves. Other mechanisms that could be implicated in the backscatter are bubbles and local wave breaking. The local wave steepness may be more significant than the spectral wave steepness. The shadowing effect at grazing incidence would be wave-height related such that larger waves (i.e., near the peak of the energy spectrum) would be enhanced relative to smaller waves. This is supported by the nonlinearity of the derived transfer function. The shadowing effect will also be related to the incidence angle. Here, we have an approximate elevation of 10 m. It seems likely that the shadowing would increase rapidly for reducing antenna elevation, especially for higher wave heights and this elevation is probably the lowest to be recommended. If the antenna height was increased to 100 m (possibly an extreme limit for a coastal deployment), the incidence angle at 700 m range would be reduced from 89.2° to 81.9°, which could have a significant effect on the amount of shadowing. This variation with elevation needs to be investigated in future deployments. From other unpublished data, it seems likely that the form of the transfer function is applicable to other similar X-band radars but more work is necessary to know how much calibration is necessary for other deployments.

A depth survey at Holderness showed evidence of an offshore bar within a few hundred meters of shore with height 2–3 m. This would be likely to broaden the spectra by spreading the energy over a wider wave number (and hence frequency) range. The depth used in the analysis does have a significant effect on the energy spectrum, although less effect on direction and spread. The main effect of an error in the depth is a shift in the frequency of the longest waves, especially important near the spectral peak. Shallower depths would lead to a shift of energy towards the lower-frequency end of the spectrum. An independent estimate of the water depth in the radar footprint is therefore desirable. Bell (1998, 1999) is working on a method for derivation of nearshore bathymetry from the radar images, which uses a completely different analysis to that for waves and is not discussed further here. This will be complementary to the wave analysis and provide further benefits from the coastal radar deployment.

7. Conclusions

The X-band radar gives useful estimates of the directional wave spectra in a coastal application. A direct estimate of the wave spectrum can be derived for frequencies 0.05–0.2 Hz. Beyond the high frequency limit, a tail-fitting procedure improves the agreement with conventional in situ wave measurement devices.

It is essential to the analysis to provide an estimate of water depth. An approximate estimate of depth can be made without external information by examination of the main spectral peak, for images with sufficient contrast (which also relates to a minimum wave height). The error in the radar-estimated depths is about ± 2 m due to the rather coarse wave number and frequency resolution. The near-range and far-range parts of the image can be analysed separately and give results consistent with expected values.

Frequency is less well resolved than wave number in this particular radar configuration. This could be improved by using a longer recording interval. Also, averaging several data samples would reduce the confidence limits on the spectral estimates.

The full mechanism of microwave radar backscatter at low (grazing) incidence is not known. An empirical transfer function between the image spectra and wave spectra has been derived here for the simultaneous WR, S4DW and radar spectra. The form of the transfer function does not agree with theory for the Bragg scattering model, but may be consistent with shadowing.

The calibration of the image spectra is likely to be applicable qualitatively in other deployments except for the overall scaling, which requires direct measurement of wave height by another means for at least some part of the time of the radar operation. More data were collected in the winter of 1995–1996. These data have not yet been processed but some improvements in the system suggest that these will be of good quality. These should be used to check the validity of the calibration. Further deployments with different antenna elevations should be made to test the portability of the transfer function.

Acknowledgements

The data were collected for the Ministry of Agriculture, Fisheries and Food under its Flood Protection Commission during the Holderness Experiment.

References

Bell, P.S., 1998. Bathymetry derived from an analysis of X-band marine radar images of waves. Proceedings of Oceanology ’98, Brighton, UK, March 1998, pp. 535–543.

Bell, P.S., 1999. Shallow water bathymetry derived from an analysis of X-band marine radar images of waves. Coastal Eng. 37 (3–4), 513–527.

Bell, P.S., Hardcastle, P.J., 1996 Combined use of an X-band Radar and an Offshore Pressure Transducer for Monitoring the Nearshore Directional Wave Climate. Proudman Oceanographic Laboratory, Internal Document no. 98, 16 pp.

Borge, J.-C.N., Reichert, K., Dittmer, J., 1999. Use of marine radar as a wave monitoring instrument. Coastal Eng. 37 (3–4), 331–342.

Heathershaw, A.D., Blackley, M.W.L., Hardcastle, P.J., 1980. Wave direction estimates in coastal waters using radar. Coastal Eng. 3, 249–267.

Krogstad, H.E., Wolf, J., Thompson, S.P., Wyatt, L., 1999. Methods for the intercomparison of wave measurements. Coastal Eng. 37 (3–4), 235–257.

Pethick, J., Leggett, D., 1993. The morphology of the Anglian Coast. In: Hillen, R., Verhagen, H.J. (Eds.), Coastlines of the Southern North Sea. American Society of Civil Engineers, New York, pp. 52–64.

Phillips, O.M., 1977. The Dynamics of the Upper Ocean. Cambridge Univ. Press, Cambridge, 336 pp.

Prandle, D., Ballard, G., Banaszek, A., Bell, P., Flatt, D., Hardcastle, P., Harrison, A., Humphrey, J., Holdaway, G., Lane, A., Player, R., Williams, J., Wolf, J., 1996. The Holderness Coastal Experiment 93–96. POL Report 44.

Proctor, R., Wolf, J., 1991. Surface wave measurements using a ship’s radar in the southern North Sea. Abstract of Paper Presented at l5th General Assembly of the European Geophysical Society, Copenhagen, 1990. Ann. Geophys., vol. 8, p. 195, 1990 Special Issue.

Reichert, K., Borge, J.-C., Dittmer, N., 1998. WaMOS II: an operational wave monitoring system. Proceedings of Oceanology ’98, Brighton, UK, March 1998, pp. 455–462.

Robinson, I.S., 1985. Satellite oceanography: an introduction for oceanographers and remote-sensing scientists. Ellis Horwood Series in Marine Sciences. Ellis Horwood, Chichester.

Tucker, M.J., 1991. Waves in Ocean Engineering: Measurement, Analysis, Interpretation. Ellis Horwood, 431 pp.

Wolf, J., 1996. The Intercomparison of Wave Data from Moored Instruments, POL Internal Document no. 103, 17 pp.

Wolf, J., 1998. Waves at Holderness: results from in situ measurements. Proceedings of Oceanology ’98, Brighton, UK, March 1998, pp. 387–398.

Wyatt, L.R., Thompson, S.P., Burton, R.R., 1999. Evaluation of HF radar wave measurement. Coastal Eng. 37, 259–282.

Young, I.R., Rosenthal, W., Ziemer, F., 1985a. A three-dimensional analysis of marine radar images for the determination of ocean wave directionality and surface currents. J. Geophys. Res. 90 (C1), 1049–1059.

Young, I.R., Rosenthal, W., Ziemer, F., 1985b. Marine radar measurements of waves and currents during turning winds. Dtsch. Hydrogr. Z. 38, 23–38.

Ziemer, F., 1991. Directional spectra from shipboard navigation radar during LEWEX. In: Beal, R.C. (Ed.), Directional Ocean Wave Spectra. Johns Hopkins Univ. Press, Baltimore, pp. 80–84, 218 pp.

Ziemer, F., Rosenthal, W., 1987. On the transfer function of a shipborne radar for imaging ocean waves. Proc. IGARSS ’87 Symp., Ann Arbor, MI, pp. 1564–1599.